High-Order Distortion in Directly Modulated Semiconductor Lasers in High-Loss Analog Optical Links With Large RF Dynamic Range

George S. D. Gordon, *Student Member, IEEE*, Michael J. Crisp, *Member, IEEE*, Richard V. Penty, *Senior Member, IEEE*, and Ian H. White, *Fellow, IEEE*

***Abstract*—A theoretical and experimental investigation of the effects of high-order nonlinear distortion products produced by directly modulated semiconductor lasers on the performance of high-loss analog optical communication links requiring large RF dynamic range is reported. In order to provide sufficient RF dynamic range to support radio services in links with high optical transmission loss, for example in radio over free-space optics (RoFSO), while keeping costs low, it is necessary to use directly modulated lasers. However, in these applications the lasers must be driven to high modulation depths to maximize dynamic range. Simulations show that under these unique conditions the first detectable nonlinear distortion is often the result of dynamic distortion due to the laser being driven near threshold. It is shown that this type of distortion is characterized by a sharp increase in the contribution of high-order (fourth order or greater) nonlinear terms resulting from the influence of laser relaxation oscillations. As a consequence, the third-order spurious-free dynamic range (SFDR) metric no longer accurately reflects the performance of such links as it assumes that third order effects are dominant. An alternative measure of dynamic range called dynamic-distortion-free dynamic range (DDFDR) is proposed. This differs in that the upper limit is defined as the modulating power at which the peak optical modulation index (OMI) reaches unity. At this point the error vector magnitude (EVM) measured for a range of different wireless services starts to increase rapidly due to high order distortion. This makes DDFDR a practical, service-independent metric of dynamic range. For two different wireless services it is observed experimentally that on average the DDFDR upper limit predicts the EVM knee point to within 1.1 dB, while the third-order SFDR predicts it to within 6.2 dB. The DDFDR is thus shown to be a more accurate indicator of real link performance when high-order distortion is dominant.**

***Index Terms*—Dynamic distortion, free-space optics, nonlinear distortion, optical modulation, spurious-free dynamic range (SFDR).**

I. Introduction

WIRELESS communications systems are an increasingly important and ubiquitous feature of modern society. With mobile data rates set to increase from 14 Mbps (3G) up to 100 Mbps (4G/LTE) it is becoming increasingly difficult to provide the required radio signal quality to users distributed over large areas. This is especially challenging in indoor environments, which is of particular concern because over 70% of mobile traffic originates indoors [1].

Better signal coverage and quality can be achieved using distributed antenna systems (DAS). Radio-over-fiber (RoF) has been shown to be a cost-effective and high-performance means of distributing broadband analog radio signals to remote antennas in DAS [2]. The fiber infrastructure requirement of RoF links can be very expensive and so in some DAS installations it may be desirable to replace them with radio over free-space optics (RoFSO) links. Such systems have been proposed for narrowband single-service cellular applications [3], [4] and also for broadband multi-service applications [5]. In order to be an economically viable alternative to a broadband RoF link, any RoFSO link must be low-cost, broadband and provide comparable performance.

Because of optical alignment tolerances, free-space loss and coupling loss, RoFSO links have to accommodate an optical loss significantly greater than RoF links. This loss will be time variant but over short periods of time can be considered to remain constant. The noise floor of these high-loss links is dominated by thermal noise in the receiver. Noise caused by scintillation is ignored because it is sufficiently low frequency (<500 Hz) and its effect is small over short distances indoors [6]. The noise figure of the link, defined as the decrease in SNR in dB, increases with the optical loss and in doing so restricts the lower limit of the RF dynamic range. In order to provide large RF dynamic range it is then necessary to push operation closer to the upper limit of the optical link RF dynamic range, which is limited by nonlinearity in the transmitter. To do this without using costly optical amplifiers or high power lasers, it is necessary to operate lasers at the maximum optical modulation depth. To keep RoFSO links relatively low-cost compared with their RoF counterparts this should be done using directly modulated semiconductor lasers as the source and a photodiode detector as the receiver.

These operating conditions make such links susceptible to high-order (i.e., greater than third order) nonlinear behavior which is generated in directly modulated semiconductor lasers as the peak OMI approaches unity, and which is called *dynamic distortion*. The effect of this behavior on the link performance is examined both theoretically and experimentally. It is found that the usual figure of merit for analog optical links, third-order

Manuscript received June 02, 2011; revised September 05, 2011, October 10, 2011; accepted October 11, 2011. Date of publication October 19, 2011; date of current version November 30, 2011. This work was supported in part by the U.K. Engineering and Physical Sciences Research Council (EPSRC).

The authors are with the Electrical Engineering Division, University of Cambridge, Cambridge CB3 0FA, U.K. (e-mail: gsdg2@cam.ac.uk; mjc87@cam.ac.uk; rvp11@cam.ac.uk; ihw3@cam.ac.uk).

Color versions of one or more of the figures in this paper are available online at http://ieeexplore.ieee.org.

Digital Object Identifier 10.1109/JLT.2011.2172773

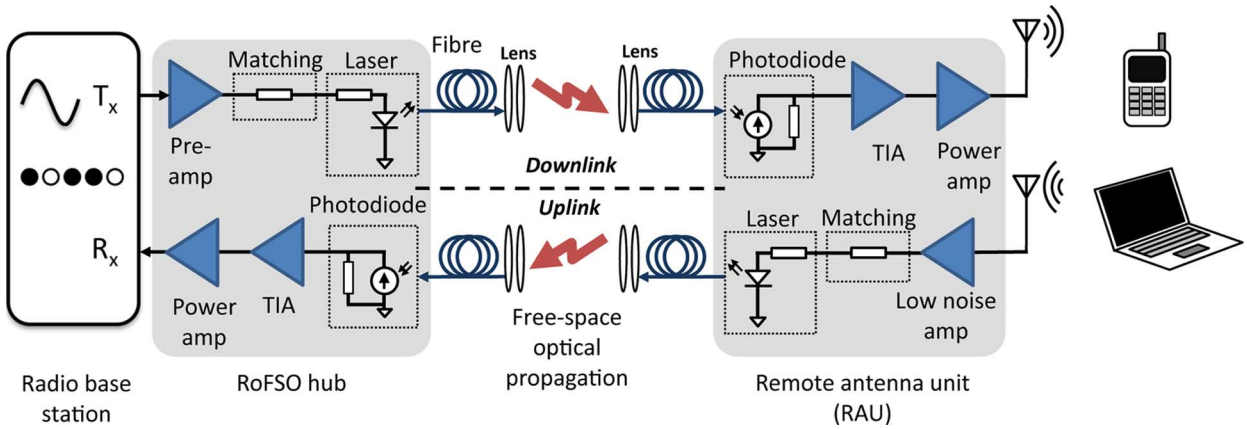

Fig. 1. Example IM-DD RoFSO system being used in a DAS.

SFDR, no longer accurately reflects the performance of such links as it assumes that third order effects are dominant. When dynamic distortion is dominant it is found that the dominant order of distortion at the input power that causes the first *intermodulation distortion* (IMD) product to be greater than the noise floor is high but not readily predictable. This is the first time that the practical implications of this high-order distortion on the performance of optical communication links have been investigated.

It is demonstrated that in such a regime a new metric called *dynamic distortion free dynamic range* (DDFDR), which is the RF dynamic range where the OMI of the laser output remains less than unity, can be a better indicator of link performance. Like third-order SFDR, DDFDR uses the noise floor as its lower limit but the upper limit uses the peak modulation power at which peak OMI reaches unity. This upper limit is bandwidth-independent and is the same regardless of the actual dominant order of distortion. At this upper limit the EVM performance of all real wireless services carried on the optical link starts to increase rapidly due to the very rapidly increasing distortion, regardless of service. The measure is thus service-independent. It is, however, only valid for systems where dynamic distortion is dominant.

An example high-RF-power high-loss optical link is used to confirm experimentally the presence of dynamic distortion and its effect on third-order SFDR, and to validate the proposed DDFDR metric. It is shown that when high-order dynamic distortion is dominant DDFDR is a better predictor of EVM performance at the onset of distortion than third-order SFDR.

II. High-RF-Power High-Loss Optical Links

Some optical links are required to run under conditions of high optical loss (or losses which are time varying and can reach high levels) compared with standard fiber links, for example links using lossy polymer optical fiber or free-space optical (FSO) links. The noise figure of such links can be calculated from the link budget if the gain and noise figure of each device are known [7]. As the optical loss increases shot noise and then thermal noise at the receiver begin to dominate. The overall noise figure of the link also increases. This restricts the lower end of the RF dynamic range because the RF signals have insufficient SNR.

To provide a large RF dynamic range to transport radio services such links must allow operation up to higher RF power levels, where distortion caused by nonlinearity imposes an upper limit. This is achieved by increasing the power of the RF modulating signal, meaning that such links can be considered high-RF-power compared to standard fiber links. Many real radio services have a high tolerance to error (for example 3GPP allows 17% EVM [8]) so can provide acceptable performance when a significant amount of nonlinearity is present. Such links can be operated at high-RF-power levels as a practical means of providing large RF dynamic range.

Free-Space Optical Links

FSO links are constructed from an optical transmitter, typically a laser, and an optical receiver, a light detector usually consisting of a focussing element and a photodiode. Such links usually transmit digital modulated signals but have been designed to support direct transmission of analog RF signals through analog RF modulation [4]. This has been achieved using a simple intensity modulation (IM) scheme at the transmitter and a simple direct detection (DD) scheme at the receiver followed by an amplifier [5]. An example IM-DD RoFSO system is illustrated in Fig. 1.

The modulation could be done using an external modulator integrated with a laser via photonic integrated circuit (PIC) technology. However, the use of external modulators is still considered to be impractical since it is more expensive than direct modulation [9]. Direct modulation of laser diodes has been shown to provide dynamic range performance comparable with externally modulated sources at lower cost [10].

1) Optical Loss in FSO Links: FSO links are prone to misalignment due to pointing error, vibrations, expansion of buildings and gradual shifting of mounts. This beam misalignment causes significant power loss and has been mitigated using automatic electromechanical tracking systems [11]. Low-cost systems requiring only manual alignment have been designed using highly divergent beams that create large beam spots at the receiver [12]. This introduces a large power loss because only a small fraction of the transmitted power is received. This loss

could be avoided with a large optical receiver but these are difficult to make.

The propagation loss for FSO links varies with time due to building movement and vibration. This variation has been shown to be relatively slow (a few kHz) compared to the bandwidths of many RF services (greater than 100 MHz) and so the loss can be considered constant over the course of a single test measurement [11]. For the same reason scintillation effects can be ignored for these short distances [6]. Using typical figures for the required beam divergence to allow for alignment error (1–5 mrad) and for the diameter of the optical receiver, the geometrical propagation loss is in the range 0.6–17 dBo [13]. Optical decibels (dBo) are used to distinguish optical power loss from RF power loss for clarity.

In addition, published experiments have found unavoidable optical coupling losses of 8–14 dBo [4], [11]. The minimum total optical loss in a FSO link with optimum alignment is therefore 8.6 dBo. By comparison, for fiber links of typical indoor DAS spans (50–100 m) the optical loss is expected to be less than 0.5 dBo in addition to laser coupling losses of 3–4 dBo. FSO links can therefore be considered to be high-loss relative to fiber links.

2) RF Transmit Power in FSO Links: Radio services must handle a large dynamic range of received powers on the uplink due to the near—far effect which must be supported by the RoFSO link. The lower end of the RF dynamic range of the RoFSO link is limited by the attenuation of low power signals and the thermal noise floor of the receiver. This could be overcome by amplifying the optical signal but optical amplifiers are too expensive for such low-cost systems. A lower-cost strategy is to increase the output power of the laser and increase the power of the RF modulating signal.

One way to do this would be to increase the bias current and output power of the laser. However, there are limits to how much laser bias levels can be increased [7]. Using a higher-powered laser would be another option but low-cost semiconductor lasers suitable for high-power direct modulation in the gigahertz frequency range are not readily available. Also, for free-space applications such as RoFSO the output power of the laser may be limited due to eye-safety requirements. Therefore, as well as increasing the optical output power to overcome the high optical losses, a high modulation depth must be used.

3) Experimental RoFSO Link: To illustrate the issues which this paper addresses, an experiment on an example of a RoFSO uplink is recorded here. The uplink as depicted in Fig. 1 is set up in an experiment to evaluate the RF dynamic range. A 16 m free-space optical link is created by coupling light to and from fibers using adjustable lenses. The laser used is a directly modulated 1310 nm Sumitomo SLV521A DFB operated at a bias current of 50 mA with a 10 mW CW output. This choice of wavelength allows the use of low-cost and readily available components. Index matching gel and optical isolators are used to prevent distortion arising from optical feedback into the laser cavity [15]. The optical loss is measured to be 10 ± 1 dBo over a 24-hour period with dynamic variations in loss being sufficiently slow that they have negligible short-term impact on performance, consistent with previous experiments [11]. The receiver used is polarisation insensitive so that changes in the orientation of the transmitter or receiver polarisation, or polarisation changes in the fiber do not affect the performance.

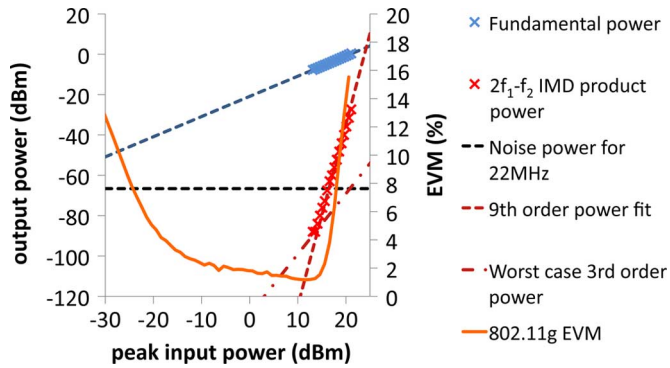

Fig. 2. Graph showing EVM versus average RF power for a demonstration RoFSO uplink.

To measure the link performance, the laser is directly modulated with a 64QAM 802.11g wireless LAN signal at a carrier frequency 2.5 GHz. The EVM versus input power curve is shown in Fig. 2. It can be seen that 38.7 dB RF dynamic range is achieved with an EVM below the 5.6% limit specified by the IEEE 802.11g standard. This demonstrates the viability of such high-loss free-space links for transporting analog RF signals as has been indicated in previous research [5].

Overlaid on the EVM curve in Fig. 2 is the power curve of the main intermodulation distortion (IMD) product arising from laser nonlinearities in a two-tone test. Due to the high peak-to-average power (PAPR) ratio of 802.11g signals the peak power of this input signal is a better indicator of the point at which distortion starts to occur. Therefore, peak power is used for all the input signals to allow a fair comparison of the onset of distortion.

It is observed that the IMD product rises above the noise floor for a 22 MHz bandwidth, (the bandwidth of the 802.11g signal), 1 dB above the peak power at which the 802.11g EVM starts to increase due to distortion, the *knee point*. This is expected because the power at which the first IMD product rises above the noise floor in a two-tone test (normalized to a service bandwidth) represents the first time distortion is large enough to cause the EVM to rise detectably above its noise-limited value.

In Fig. 2 this IMD product does not follow a third-order trend. However, it is expected that at low powers third-order distortion would dominate. Therefore, a 'worst case' third-order fit, assuming third order behavior ceases immediately below the instrument noise floor, is used. When this is extrapolated it is found that its intercept with the 22 MHz bandwidth noise floor is 8 dB above the EVM knee point. Evidently the common assumption of a third-order dominated IMD product, which can be extrapolated to predict the dynamic range at a particular bandwidth, is not accurate here.

The measured IMD products suggest that high-order (5th and greater) nonlinearities are dominant. Consequently, third-order SFDR no longer accurately reflects performance under modulation with real signals because it assumes nonlinearity is third-order dominated. An alternative metric is needed to enable design and comparison of links.

III. Nonlinear Behavior in Lasers

As shown in the previous section, high-order nonlinear distortion can arise in RoFSO links as a result of the high optical loss and the high modulation depths used. In order to develop a new metric to quantify dynamic range when third-order SFDR fails it is necessary to understand theoretically the causes of this high order distortion at high modulation depths and to simulate this behavior.

A. Causes of Nonlinearity

Models for the behavior of directly modulated semiconductor lasers are well-established [16]. In order to investigate nonlinearity it is necessary observe how such a model behaves under extreme modulation conditions. Previous research into dynamic distortion has successfully used a simple rate equation model and so a similar approach is used here [17]:

$$\frac{dN}{dt} = \frac{I}{eV} - g_0(N - N_{om})(1 - \varepsilon P) - \frac{N}{\tau_n}$$
$$\frac{dP}{dt} = \Gamma g_0(N - N_{om})(1 - \varepsilon P)P - \frac{P}{\tau_p} + \Gamma\beta\frac{N}{\tau_n}$$

where N represents the carrier density, N_{om} the transparency carrier density, I the drive current of the laser, e the unit charge, V the volume of the active region, g_0 the optical gain, P the photon density, ε the gain compression factor, Γ the confinement factor, β the spontaneous emission coupling coefficient, τ_p the photon lifetime and τ_n the carrier lifetime.

A third equation representing the optical phase of the light inside the cavity is commonly used. However, the theoretical results derived here are for devices intended to be used in optical links using phase-insensitive photodiode intensity envelope detectors. Similarly, the intended links for these devices are sufficiently short that dispersion can be neglected and do not use narrowband optical filtering so there is no mechanism for FM-IM conversion. As a result optical phase can be omitted from the simulation for simplicity. The simulated behavior matches closely that observed experimentally in Section IV, indicating the validity of this assumption.

These rate equations are solved for a number of different drive currents using the following parameters, taken from related work on simulating nonlinear effects in semiconductor lasers [15]: $N_{om} = 4.6 \times 10^{24}$ m^{-3}, $eV = 1.44 \times 10^{-35}$ m^{3}C, $g_0 = 10^{-12}$s^{-1} m^3, $\varepsilon = 3.8 \times 10^{-23}$ m^3, $\Gamma = 0.646$, $\beta = 10^{-3}$, $\tau_p = 2$ ps, $\tau_n = 3.72$ ns, $I_{\rm th} \sim 21$ mA. Additional parameters used in the simulation are the effective refractive index of the laser cavity, $n_{\rm eff} = 3.6$, wavelength of light, $\lambda = 1310$ nm, reflectivity of the cavity ends, $R = 0.2985$, cavity length, $L = 300$ μm, bias current, $I_{\rm bias} = 110$ mA, and conversion ratio of the photodiode receiver, $G = 450$ V/W. Although changes in temperature can alter the threshold current, gain and wavelength of the laser, creating potential additional nonlinearity [18], the temperature is assumed to be constant. The 1310 nm wavelength is chosen to leverage the availability of low-cost lasers designed for 10 GbE and better system margins when compared with 850 nm devices.

In directly modulated lasers, nonlinear effects become more significant as the *optical modulation index* (OMI) increases. OMI can be quoted as an RMS quantity but in this paper the terms OMI and *peak* OMI are used interchangeably to mean the maximum instantaneous OMI. Therefore, for a single tone input the OMI is defined as $\text{OMI} = I_{\rm amp}/(I_{\rm bias} - I_{\rm th})$. For other input signals the maximum instantaneous current replaces $I_{\rm amp}$.

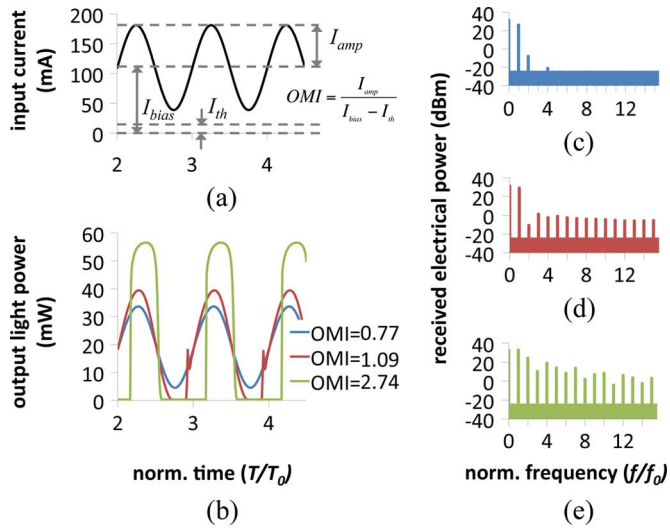

Fig. 3. Simulation results illustrating different types of distortion: (a) input current consisting of a bias current, $I_{\rm bias}$, of 110 mA and a modulating sinusoid at frequency $f_0 = 1$ GHz ($T_0 = 1$ ns) with an amplitude, $I_{\rm amp}$, of 72 mA resulting in an OMI of 0.77 (b) laser output power versus time showing the effects of static, dynamic and overmodulation distortion encountered for $\text{OMI} = 0.77, 1.09$ and 2.74 respectively, (c)–(e) power spectra of the received electrical signals for the static, dynamic and overmodulation distortion scenarios respectively.

Consider the case of a laser biased well above the lasing threshold and modulated with single frequency sinusoid. If the OMI is less than unity, then a small amount of nonlinearity will arise from the gain compression factor ε. This gain compression is a result of a number of effects including gain saturation due to a finite number of carriers, spatial hole burning and leakage currents [18]. Nonlinearity in this regime that arises primarily from gain compression is termed *static distortion*, as illustrated in Fig. 3, and is typically dominated by second-order and third-order effects.

As the OMI rises to unity the minimum drive current begins to drop just below the laser threshold current and a second type of nonlinearity caused by the turn-on delay begins to occur. This sudden turning on of the laser can be modelled accurately using fairly simple approximations [19]. However, the rate equation model is necessary to simulate additional nonlinear effects caused by relaxation oscillations. This is referred to as *dynamic distortion*, as illustrated in Fig. 3.

As OMI increases even further gain compression starts to damp the relaxation oscillations caused by dynamic distortion thereby reducing its effect. This also limits the maximum output power. Thus, the output power is effectively clamped at both upper and lower limits creating a clipped sine-wave. Nonlinearity in this regime is referred to as *overmodulation distortion*, as illustrated in Fig. 3.

The frequency domain spectra for static, dynamic and overmodulation distortion scenarios are shown in Fig. 3. It can be seen that high-order harmonics (5th order and above) are barely detectable in the static distortion regime, but become more prominent when dynamic distortion begins to occur. Previous

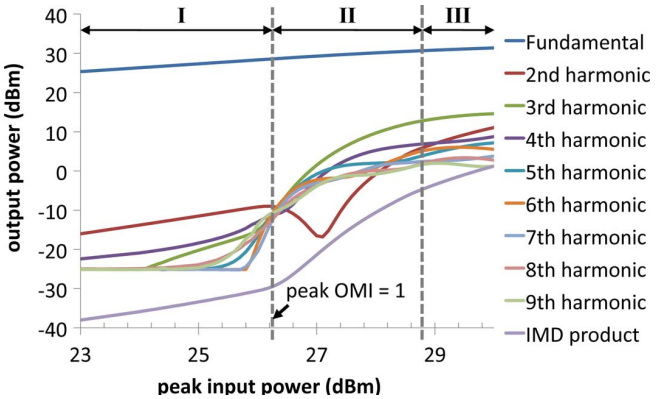

Fig. 4. Graph showing how power of harmonics varies as peak input power (or equivalently OMI) is increased for a single-tone input. The three regimes of distortion are indicated on the graph. I: static distortion; II: dynamic distortion; III: overmodulation. Also shown is the power of the $2f_1 - f_2$ IMD resulting from a two-tone input.

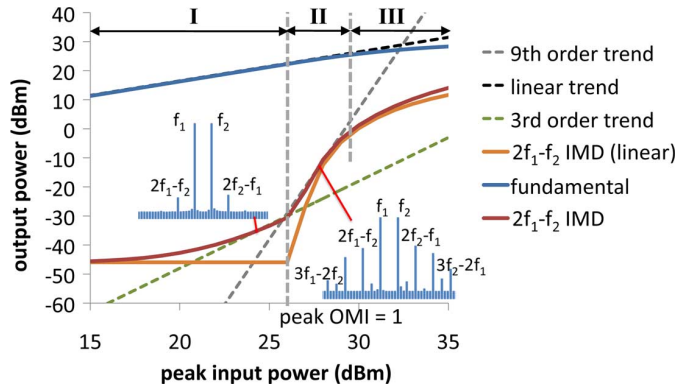

Fig. 5. Graph of output power versus peak input power for a two-tone input with tones at 950 MHz and 1.05 GHz. The three regimes of distortion are indicated on the graph. I: static distortion; II: dynamic distortion; III: overmodulation distortion. The curve labelled 'linear' shows the case when the gain compression factor is zero. Overlayed are the spectra of the received electrical power showing the magnitudes of the various IMD products, including higher order products such as $3f_1 - 2f_2$.

work has shown significant spectral broadening due to FM effects under large OMI conditions but in this case only IM effects need to be considered [20].

The powers of the first 9 harmonics are recorded as the input power, or equivalently the OMI, is increased and are plotted in Fig. 4. It can be seen that at the point where the OMI reaches unity, dynamic distortion begins to occur and the higher order harmonics increase rapidly in power. Prior to this point, in the static distortion regime, only the first four harmonics are significant. This shows that dynamic distortion is dominated by high-order nonlinear effects.

Previous research has shown that the relaxation oscillations occurring in this regime create increased levels of distortion, but this is the first time a link between this effect and increased high-order distortion has been drawn [17], [21]. Static distortion can be reduced through use of predistortion circuits but these are undesirable for RoFSO as they only cancel up to third-order distortion and have narrow operating bandwidths [22].

B. Effects on Third-Order SFDR

In high-loss optical links it is often the case that dynamic distortion has already started to occur in the laser before the first IMD product becomes greater than the noise floor. In this case dynamic distortion is the dominant factor determining RF dynamic range.

Previous research has investigated the effects of third-order IMD products on the third-order SFDR of analog optical links using a range of different lasers [23]. However, as will be shown, these methods of analysis become less meaningful when the laser is driven at high OMI as the dominant order of the distortion is not readily predictable. Work has also been conducted on DFB lasers as standalone devices and their performance under modulation in analog applications, particularly CATV [24]. However, they only examine static distortion effects and do not consider the effects of high-order dynamic distortion on third-order SFDR or on performance metrics used for real services under high optical loss.

The nonlinear distortion in any of the three regimes can be considered to arise from a high-order polynomial transfer function. For a two-tone input, consisting of tones at frequencies f_1 and f_2, it can be shown that the $2f_1 - f_2$ IMD product is contributed to by all odd order polynomial terms as follows:

$$P_{2f_1-f_2} = a_3\frac{3}{4}A^3 + a_5\frac{25}{8}A^5 + a_7\frac{735}{64}A^7 + a_9\frac{1323}{32}A^9 + \cdots$$

where P_{2f1-f2} is the power of the first IMD product, A is the amplitude of the current of a single input tone and a_n is the Taylor series coefficient for the nth order term of the polynomial light–current transfer function of the laser. In many systems third-order distortion dominates and so the fifth and higher order terms are neglected. When dynamic distortion is dominant, however, the high-order terms contribute significantly to the first IMD product.

Using the same parameters described in the previous section, the power of the first IMD product with increasing input drive power is simulated. The result is shown in Fig. 5.

It can be seen that the first IMD product begins to rise above the noise floor with a slope of 3, indicating the initial dominance of third-order nonlinearity. When the peak OMI reaches unity the curve for the first IMD product undergoes a sharp increase in slope. This point coincides with the sharp increase in power of higher order harmonics as was shown in Fig. 4. This change in slope of the IMD product power curve can then be seen to be due to increased levels of high-order distortion created by dynamic distortion. The slope observed is much greater than 3 but is not constant or predictable (in Fig. 5 it reaches a maximum value of 9). The dominant order of distortion at any power level is unpredictable without precise knowledge of the laser parameters, which are not often available. As the input power is further increased overmodulation distortion starts to dominate and the IMD product power begins to roll off.

For any nonlinear system it is expected that as power is increased higher order effects will become noticeable at some point. However, previous research has clearly identified a link between the presence of relaxation oscillations and a sudden change in nonlinear behavior as the OMI approaches unity [21]. These relaxation oscillations cause nonlinear behavior of a higher order than would be expected in the case of a clipped sinusoid exhibiting no high-frequency oscillatory behavior, which is often the assumed behavior for systems operating in a

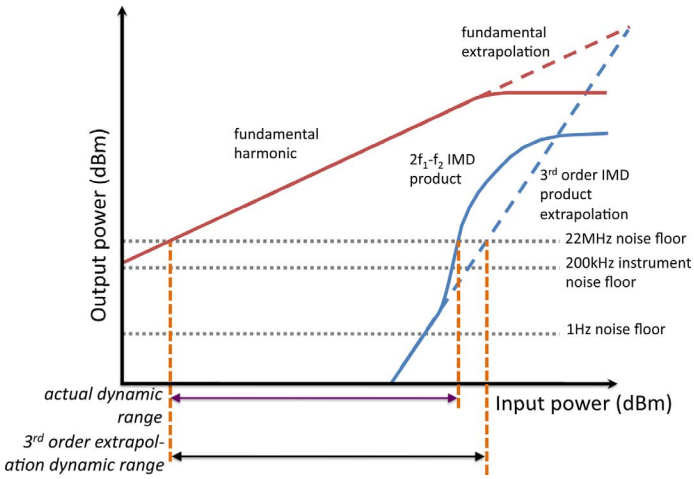

Fig. 6. Schematic graph showing received electrical output power versus input power of a single tone for a two-tone test.

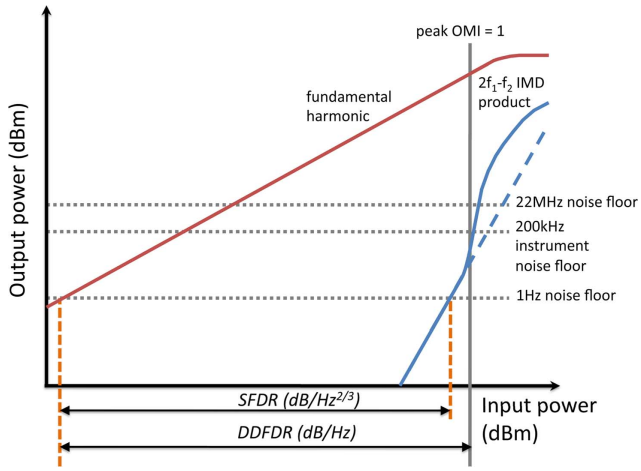

Fig. 7. Illustration of normalized DDFDR metric with an upper power limit at the point where OMI = 1. Also shown is the 1 Hz normalized third-order SFDR, valid only at small bandwidths. 22 MHz is the bandwidth of 802.11g wireless.

clipping regime. This high-order behavior will occur even for a theoretical perfectly linear laser that does not exhibit any gain compression as shown in Fig. 5.

The third-order SFDR is measured in a two-tone test where the input power of the tones is increased until a third-order trend line can be established. This third-order trend is then extrapolated to lower powers to find the intercept with the 1 Hz noise floor as shown in Fig. 6, giving the 1 Hz normalized third-order SFDR. This can then be used to estimate the useful dynamic range of a service with a particular bandwidth by extrapolating the third-order trend to higher powers and finding the intercept of the trend with the noise floor at that bandwidth assuming that the dominant distortion will remain as third-order. However, this assumption is invalid in the systems described here because under dynamic distortion higher order effects dominate. It is therefore not possible to perform the usual linear extrapolation and so the 1 Hz normalized SFDR figure is no longer a useful indicator of the dynamic range at a given bandwidth.

If this is ignored and the standard third-order extrapolation from the 1 Hz noise floor is used anyway it will tend to overestimate the distortion-free dynamic range at higher bandwidths (with their associated higher noise floors). For example the third-order SFDR overestimation for a 22 MHz bandwidth noise floor, as used for 802.11g wireless services, is shown in Fig. 6.

However, third-order SFDR is still an attractive figure of merit because it is can determined using a simple test that can be run independently of any particular service and at any frequency, or can be calculated from measurable device parameters. It is also a commonly used metric and so is important for comparison purposes. However, since the dominant order of the distortion under deep modulation with a high noise figure cannot be predicted another service-independent measure of the performance limits for directly modulated high-RF-power high-loss optical links that retains the desirable properties of third-order SFDR is needed.

C. Dynamic Distortion Free Dynamic Range

When dynamic distortion is dominant, there is a very steep increase in the power of the first IMD product just after the peak OMI reaches unity. The slope of the IMD product curve at this point is unknown and constantly changing but is large (usually above 7th order). This is sufficiently steep that it can be modelled by a vertical line at the input power for which $\mathrm{OMI} = 1$. This sets an upper limit on the peak RF modulating power that is independent of bandwidth and the exact order of distortion.

It is predicted that this sharp rise in distortion causes a sharp increase in EVM for a radio service sent over the link when the RF modulating power is such that the peak OMI reaches unity. This should cause the knee point of any EVM versus power curve to occur at the same peak power regardless of service. RF services can continue to operate beyond the knee point as they are designed to cope with some third-order distortion. However, when high-order distortion is dominant EVM increases more rapidly so the knee point becomes a good indicator of a practical upper limit for the RF modulating power. The RF power where peak OMI is unity is therefore a realistic and practical measure of the highest modulating power that can be used when dynamic distortion is dominant.

Aside from increasing EVM due to in-band interference, distortion also causes out-of-band interference. However, due to the availability of robust means to deal with this interference, EVM is almost always the first metric to deviate from the required standard as signal power is increased [25].

It is proposed that a new measure of dynamic range called *dynamic distortion free dynamic range* (DDFDR) be used as a measure of dynamic range under dynamic distortion dominated conditions. The upper limit of this is defined as the RF modulating power at which the peak $\mathrm{OMI} = 1$ and the lower limit is defined as the RF modulating power at which the $\mathrm{SNR} = 1$ for a given bandwidth. This is illustrated in Fig. 7. The point where peak $\mathrm{OMI} = 1$ can easily be calculated from the device parameters of the laser, which is simpler than finding the third-order intercept required for third-order SFDR. The noise can be calculated for a link using device parameters of all the components, as is done for third-order SFDR. Like third-order SFDR, DDFDR can be normalized to a 1 Hz bandwidth. In most situations DDFDR would not be valid at a bandwidth of 1 Hz and third-order SFDR would be a more suitable metric due to

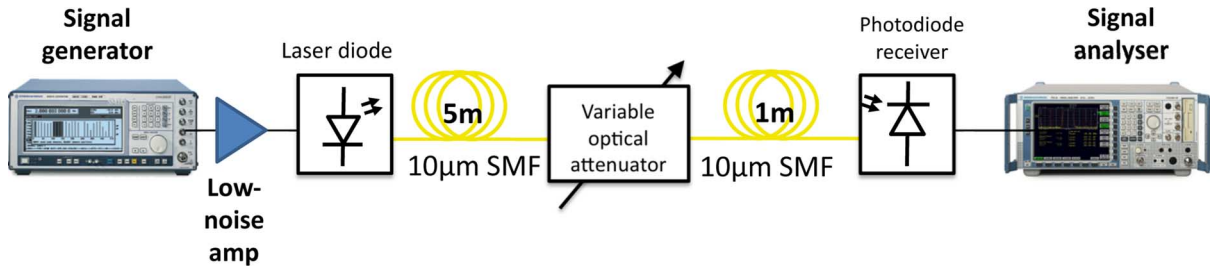

Fig. 8. Experimental setup used for testing of RoF link.

TABLE I
PARAMETERS FOR EXPERIMENTAL SETUP

Parameter	Specification
laser part number	Sumitomo SLV521A DFB
wavelength	1310 nm
CW transmit power	10 dBm
laser bias current	50 mA
optical attenuator loss	11.9dBo
photodiode receiver	Agilent 11982A Amplified Lightwave Converter
tested modulation frequency	2.5 GHz
laser operating temperature	25° C
noise measurement bandwidth	200 kHz
peak OMI range	0.1-3.5

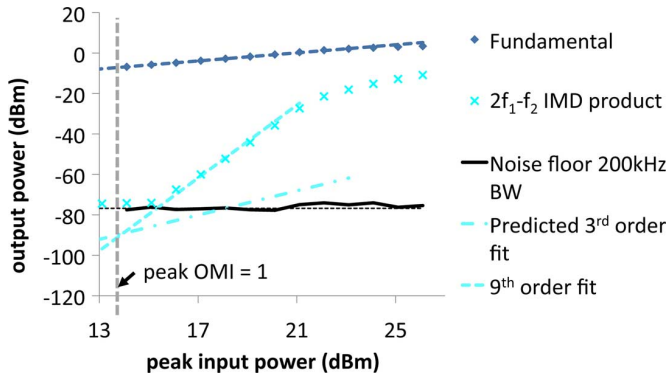

Fig. 9. Graph showing output power versus peak input power for a two-tone SFDR test with the 1310 nm Sumitomo SLV521A DFB.

dominant third-order behavior in this regime. However, normalisation allows the DDFDR to be calculated for a service of any bandwidth and for comparison between links. The units of normalized DDFDR are dB/Hz and so to find the DDFDR for a particular bandwidth it is necessary to add the bandwidth in dB to the normalized figure.

DDFDR is only accurate if the noise figure is sufficiently high that the first IMD product intercepts the noise floor after the peak OMI of the modulating signal reaches unity and if high-order dynamic distortion is dominant at this point. In the case of RoFSO links this high noise figure can be due to high optical loss or high bandwidth services. For noise figures lower than this third-order static distortion is usually dominant and third-order SFDR can be used accurately.

DDFDR has a tendency to underestimate actual dynamic range as the upper limit is less than the actual IMD product power. However this is desirable when designing systems as it provides a worst case scenario.

IV. EXPERIMENTAL INVESTIGATION

To verify the theoretical results presented in the previous section it is shown that high-order distortion effects are experimentally reproducible in directly modulated lasers with high-modulation depths and that in high-loss optical links this reduces the utility of third-order SFDR. Further, the DDFDR of the laser used is shown to be a better predictor of link EVM performance under such conditions.

A. Setup

For this experimental investigation a high-RF-power high-loss IM-DD RoF test link is used, as shown in Fig. 8. The parameters for this setup are listed in Table I.

An optical attenuator is used to allow variable optical loss. The results in the next section using this attenuator show a good match with the results in Section II using an actual free-space link. For the photodiode used, the maximum allowable optical input power is 2 dBm and so the attenuation is set to ensure that the received optical power is far enough below this to avoid causing further nonlinear distortion.

The temperature is held at 25 °C using a TEC. Dynamic temperature effects only become important at modulation frequencies less than 100 MHz and so do not affect temperature stability here [18].

B. High-Order Dynamic Distortion

For the experimental setup described previously the power of the first IMD product in a two-tone test is measured and is plotted against input power as shown in Fig. 9.

It can be seen that the first IMD product does not exhibit third-order behavior—a ninth-order slope provides a better fit. Because of the high optical loss of this link even for an RF bandwidth as low as 200 kHz, the first effect to appear above the noise floor is this high-order distortion. Using the third-order extrapolation technique discussed in Section III, for a bandwidth of 22 MHz (used in 802.11g) the calculated third-order SFDR is at least 6 dB larger than the actual IMD product free dynamic range.

When the spectrum is analyzed, as shown in Fig. 10, the IMD products created exclusively by fifth and higher order distortion products are present. Clearly, high-order nonlinearities are dominant in this case and their appearance is consistent with the onset of dynamic distortion as predicted in Section III. With this particular link it is not possible to observe third-order distortion

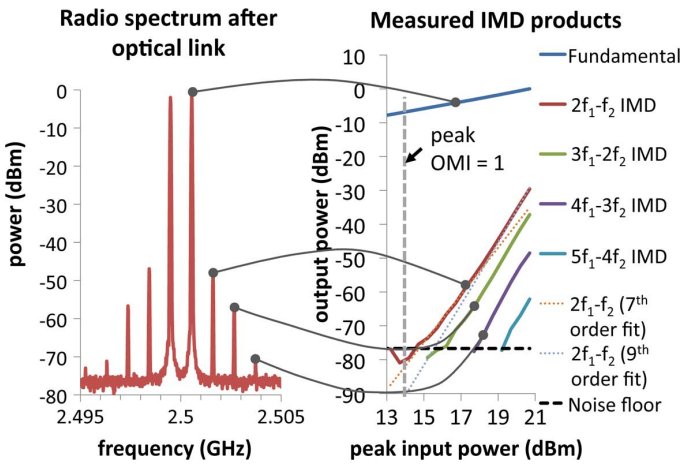

Fig. 10. Graph showing high-order IMD products at output of test link under a two-tone test. The plot on the left is the spectrum and the plot on the right shows how the different components increase with input power.

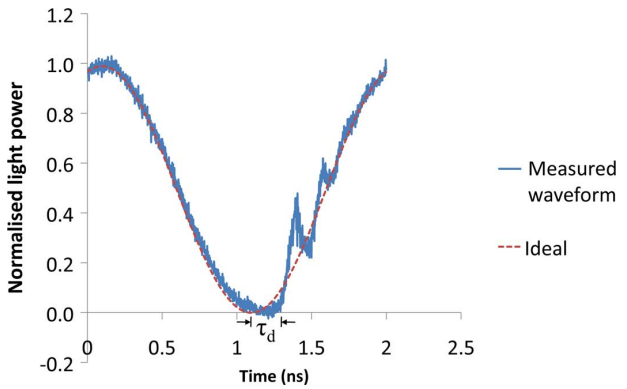

Fig. 11. Measured graph of light power versus time showing turn-on delay, τ_d, followed by relaxation oscillations, both hallmarks of dynamic distortion.

by reducing optical loss because any further decrease in optical loss begins to cause nonlinear behavior in the photodiode.

The measured time domain response of the link with a single tone input at 500 MHz is shown in Fig. 11. It can be seen that for this particular modulation level the laser drive current drops below the threshold and when it turns on again there is a delay followed by relaxation oscillations. This is the behavior predicted in Section III and is the cause of dynamic distortion.

Two other lasers are also tested under similar conditions. Optical losses are kept the same but transmit powers and bias currents are adjusted in order to run the lasers at their optimum operating points. The test conditions are still representative of RoFSO systems. The plots for the two-tone SFDR tests are shown in Figs. 12 and 13.

For both of these lasers, the first nonlinear behavior to be observed is third-order. However, in both cases the noise floor appears very close to the onset of high-order distortion meaning that if higher optical loss or higher RF bandwidth are used the high-order distortion will dominate. For example, in both cases high-order distortion would become dominant with 5 dBo additional optical loss and a 2 MHz signal bandwidth. It can be seen that this dominance of dynamic distortion is not a consequence

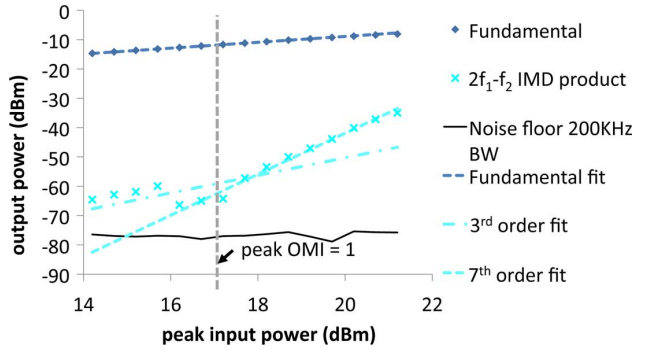

Fig. 12. Graph showing output power versus input power for two-tone SFDR test using a 1547 nm Mitsubishi FU-68PDF DFB at 9.45 dBm output power and 50 mA bias current.

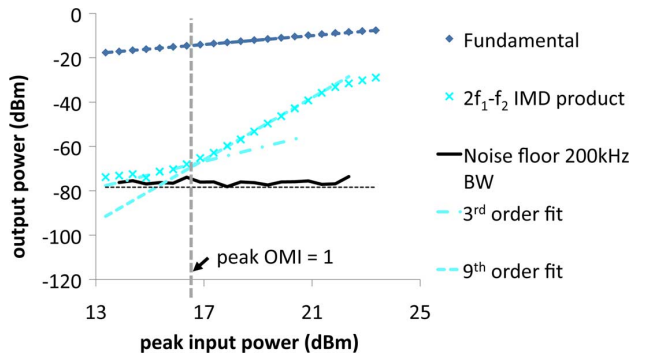

Fig. 13. Graph showing output power versus input power for two-tone SFDR test using a 1310 nm Sumitomo SLW4260 DFB at 4.94 dBm output power and 40 mA bias current.

of the particular laser used. Rather, the operating conditions of high-RF-power, high-loss, RoFSO links, make them very susceptible to it.

It is also noted that the dominant order of distortion varies between the lasers—7th order is a good fit for the 1547 nm laser while 9th order is better for the 1310 nm device. This demonstrates the dependence on measurement conditions of the order of distortion in these high-order cases. This agrees with the theory proposed in Section III.

From a practical perspective it is undesirable to drive the laser sufficiently hard that dynamic distortion is encountered. However, in order to use the maximum RF dynamic range it is necessary to be able to establish limits for linear operation. Third-order SFDR is not suitable for this task in cases where high-order effects are dominant so DDFDR provides a more accurate and realistic alternative.

As far the authors are aware this is the first practical situation in which dynamic distortion effects have been found to be important and the first time their impact on third-order SFDR and modulation performance has been investigated.

C. DDFDR Performance

To examine the performance of the DDFDR a two-tone test is performed using the same link setup with the 1310 nm laser described in the previous section. EVM curves for 802.11g and

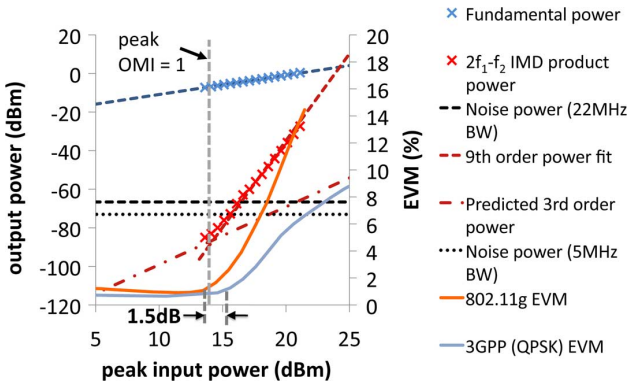

Fig. 14. Graph showing comparison of two-tone SFDR power curve and EVM curves for several modulation schemes at 2.5 GHz. Solid curves represent EVM values while dashed curves represent output power levels for a two-tone test.

TABLE II
OFFSETS OF THIRD-ORDER SFDR AND DDFDR UPPER LIMITS FROM EVM KNEE POINTS

Service	Offset of knee point from SFDR upper limit	Offset of knee point from DDFDR upper limit
802.11g	-8.4dB	-1.5dB
3GPP	-4.1dB	0.7dB

3GPP services over the same link are also recorded and the results overlaid in Fig. 14.

Both tests use the 2.5 GHz carrier frequency. The 3GPP service is tested in QPSK modulation mode. The 802.11g service is tested in 54 Mbps 64QAM mode. When comparing EVM for different modulation schemes the peak OMI is defined using statistical measures of the *peak to average power ratio* (PAPR). Measurements have shown that for 802.11g instantaneous power is less than 10 dB above the average 99.9% of the time [25]. Similar statistical values can be obtained for a two-tone SFDR test signal and 3GPP [26], [27]. This allows for a fair comparison between services.

It is observed that both the services tested reach their knee points and experience an increase in EVM at the same peak input power of 14 dBm. This is the point at which the peak OMI of these services reaches unity. The overlay of the IMD product indicates that high-order dynamic distortion is the dominant nonlinear effect in this setup. This is consistent with the theory that the high-order behavior of the IMD product curve is linked to this abrupt increase in EVM across all the services as proposed in Section III.

For each service, the knee point of the EVM curve is compared with the DDFDR upper limit and the third-order SFDR upper limit for the service bandwidth (22 MHz for 802.11g and 5 MHz for 3GPP). The offset of the DDFDR and SFDR upper limits from the EVM knee points are shown in Table II.

It can be seen that the DDFDR upper limit gives a more accurate estimate of the EVM knee point than SFDR. Across the two services the average magnitude of the offset of the DDFDR upper limit from the knee point is 1.1 dB while for third-order SFDR it is 6.2 dB. This result suggests that DDFDR provides a more accurate and realistic estimate of RF dynamic range than third-order SFDR for real services under conditions where high-order dynamic distortion of unknown order is dominant.

The knee points of the services have a spread of 1.5 dB showing that the upper limit of the DDFDR metric denotes the power beyond which high-order distortion starts to significantly degrade EVM performance, irrespective of the actual service tested thus making it service-independent. Knowing the DDFDR allows such links to be designed to avoid this high-order distortion regime.

V. CONCLUSION

It is shown theoretically and experimentally that dynamic distortion tends to be the dominant factor limiting performance in high-RF-power high-loss analog optical links using directly modulated semiconductor lasers, such as low-cost RoFSO links. Dynamic distortion is caused by relaxation oscillations and hence characterized by high-order nonlinear effects. It is shown that due to their operating conditions, high loss links are susceptible to this dynamic distortion.

In order to demonstrate a link's ability to support radio services it is necessary to use a service- and bandwidth-independent measure of dynamic range. Usually this is achieved using third-order SFDR but this fails in these situations due to the dominant high-order distortion. It is not possible to use a higher order equivalent of SFDR because the exact order of the distortion is unknown. A new measure of dynamic range, dynamic distortion free dynamic range (DDFDR) is proposed, the upper power limit of which is the RF power at which the peak instantaneous OMI reaches unity. The lower limit is the noise floor power, similar to third-order SFDR. DDFDR can be bandwidth normalized, like third-order SFDR, but is only valid under conditions where high-order distortion is dominant. DDFDR can be evaluated at a range of different frequencies to demonstrate the broadband and service-independent operation of a system. It can also be used to compare between different lasers in the same link.

It is observed that when the peak OMI reaches unity in high-RF-power high-loss optical links the EVM of a number of services increases at the same peak power level, independent of bandwidth or modulation scheme. This causes an effective compression of the knee points for the EVM curves across different services. It is found experimentally that when EVM curves for different services are compared the knee points all fall within a 1.5 dB range of one another irrespective of the RF service. Further, it is shown experimentally that in dynamic distortion limited systems the upper limit of the DDFDR can on average predict the EVM knee point to within 1.1 dB, compared to third-order SFDR which only predicts it to within 6.2 dB. This indicates that under conditions of dominant dynamic distortion the DDFDR provides a better service-independent indicator of the limits within which a link can be operated without experiencing increased EVM than third-order SFDR.

ACKNOWLEDGMENT

The authors would like to thank A. Wonfor for his helpful advice. They would also like to thank the U.K. Engineering and Physical Sciences Research Council (EPSRC) and the Rutherford Foundation of the Royal Society of New Zealand for their support.

REFERENCES

[1] C. Chevallier *et al., WCDMA UMTS Deployment Handbook*. Chichester, U.K.: Wiley, 2006, p. 316.

[2] P. Hartmann, X. Qian, R. Penty, and I. White, "Broadband multimode fibre (MMF) based IEEE 802.11a/b/g WLAN distribution system," in *Proc. IEEE Int. Top. Meeting Microw. Photon.*, Ogunquit, ME, 2004, pp. 173–176.

[3] G. Katz, S. Arnon, P. Goldgeier, Y. Hauptman, and N. Atias, "Cellular over optical wireless networks," *Proc. Inst. Elect. Eng.—Optoelectron.*, vol. 153, p. 195, 2006.

[4] H. H. Refai, "Transporting RF signals over free-space optical links," in *Proc. SPIE*, 2005, vol. 5712, pp. 46–54.

[5] G. S. D. Gordon, M. J. Crisp, R. V. Penty, and I. H. White, "Demonstration of a low-cost broadband radio over free- space optics system," presented at the Semiconductor and Integrated Optoelectron. Conf., Cardiff, U.K., 2010.

[6] R. S. Lawrence and J. W. Strohbehn, "A survey of clear-air propagation effects relevant to optical communications," *Proc. IEEE*, vol. 58, no. 10, pp. 1523–1545, Oct. 1970.

[7] C. H. I. Cox, *Analog Optical Links—Theory and Practice*. New York: Cambridge Univ., 2005.

[8] ETSI TS 125 141 V9.4.0 (2010-07) Technical Specification Universal Mobile Telecommunications System (UMTS); Base Station (BS) Conformance Testing (FDD) 2010, 3GPP Technical Specification 25.141 version 9.4.0 Release 9.

[9] D. A. I. Marpaung, C. G. H. Roeloffzen, and W. C. van Etten, "A broadband high dynamic range analog photonic link using push-pull directly-modulated semiconductor lasers," in *IEEE MTT-S Int. Microw. Symp. Dig.*, 2008, pp. 507–510.

[10] C. H. Cox, E. I. Ackerman, G. E. Betts, and J. L. Prince, "Limits on the performance of RF-over-fiber links and their impact on device design," *IEEE Trans. Microw. Theory Tech.*, vol. 54, no. 2, pp. 906–920, Feb. 2006.

[11] E. Ciaramella *et al.*, "1.28 Terabit/s (32 × 40 Gbit/s) WDM transmission system for free space optical communications," *IEEE J. Sel. Areas Commun.*, vol. 27, no. 9, pp. 1639–1645, Dec. 2009.

[12] A. Acampora, S. H. Bloom, and S. Krishnamurthy, "UniNet: A hybrid approach for universal broadband access using small radio cells interconnected by free-space optical links," *IEEE J. Sel. Areas Commun.*, vol. 16, no. 8, pp. 973–987, Aug. 1998.

[13] I. I. Kim, R. Stieger, J. Koontz, C. Moursund, M. Barclay, P. Adhikari, J. Schuster, E. Korevaar, R. Ruigrok, and C. De Cusatis, "Wireless optical transmission of fast Ethernet, FDDI, ATM, and ESCON protocol data using the TerraLink laser communication system," *Opt. Eng.*, vol. 37, pp. 3143–3155, Dec. 1998.

[14] C. H. I. Cox, *Analog Optical Links—Theory and Practice*. New York: Cambridge Univ., 2005.

[15] J. Helms, "Intermodulation and harmonic distortions of laser diodes with optical feedback," *J. Lightw. Technol.*, vol. 9, no. 11, pp. 1567–1575, Nov. 1991.

[16] S. Ghoniemy, L. MacEachern, and S. Mahmoud, "Extended robust semiconductor laser modeling for analog optical link simulations," *IEEE Journal of Selected Topics in Quantum Electronics*, vol. 9, no. 3, pp. 872–878, May 2003.

[17] M. K. Haldar, K. B. Chia, and F. V. C. Mendis, "Dynamic considerations in overmodulation of semiconductor laser diodes," *Electron. Lett.*, vol. 32, no. 7, pp. 659–661, Mar. 1996.

[18] G. Morthier and P. Vankwikelberge, *Handbook of Distributed Feedback Laser Diodes*. Norwood, MA: Artech House, 1997.

[19] J. L. Bihan, "Approximate dynamic model for evaluating distortion in a semiconductor laser under overmodulation," *IEEE Photon. Technol. Lett.*, vol. 9, no. 3, pp. 303–305, Mar. 1997.

[20] I. Vurgaftman and J. Singh, "Dynamic instabilities in the power spectrum of deeply modulated semiconductor lasers," *J. Appl. Phys.*, vol. 76, no. 7, p. 4003, 1994.

[21] B. H. Wang and W. I. Way, "Large-signal spurious-free dynamic range due to static and dynamic clipping in direct and external modulation systems," *J. Lightw. Technol.*, vol. 16, no. 10, Oct. 1998.

[22] L. Roselli *et al.*, "Analog laser predistortion for multiservice radio-over-fiber systems," *J. Lightw. Technol.*, vol. 21, no. 5, pp. 1211–1223, May 2003.

[23] T. Marozsak, A. Kovacs, E. Udvary, and T. Berceli, "Direct modulated lasers in radio over fiber applications," in *Proc. Int. Top. Meeting Microw. Photon.*, Awaji, Japan, 2002, pp. 129–132.

[24] H. Yonetani, I. Ushijima, T. Takada, and K. Shima, "Transmission characteristics of DFB laser modules for analog applications," *J. Lightw. Technol.*, vol. 11, no. 1, pp. 147–153, Jan. 1993.

[25] D. M. Dobkin, *RF Engineering for Wireless Networks: Hardware, Antennas, and Propagation*. Boston, Mass.: Newnes, 2005, pp. 126–144.

[26] P. Cruz and N. B. Carvalho, "PAPR evaluation in multi-mode SDR transceivers," in *Proc. 38th Eur. Microw. Conf.*, Amsterdam, The Netherlands, 2008, pp. 1354–1357.

[27] R. L. Abrahams, "Troubleshooting dual-band WLAN radios," Wireless Systems Design Mar. 2003 [Online]. Available: http://www.wsdmag.com/Articles/ArticleID/6578/6578.html, [Online]. Available

George S. D. Gordon (S'06) received the B.Eng. (Hons.) degree in electrical and electronics engineering from the University of Auckland, Auckland, New Zealand, in 2009. He is currently working toward the Ph.D. degree in electrical engineering at the University of Cambridge, Cambridge, U.K., under the supervision of Prof. Ian White.

His research interests include radio over fiber distributed antenna systems and multiple-input multiple-output antenna systems and their application to improving wireless services in indoor environments.

Michael J. Crisp (M'09) received the M.Eng. degree and Ph.D. degree in engineering for research on radio over fiber systems and distributed antenna systems from the University of Cambridge, Cambridge, U.K., in 2005 and 2009, respectively.

He is currently a Postdoctoral Research Associate with the University of Cambridge, Cambridge, U.K., working on RFID distributed antenna systems and radio-over-fiber systems.

Richard V. Penty (M'00–SM'10) received the Ph.D. degree in engineering for his research on optical fiber devices for signal processing applications from the University of Cambridge, Cambridge, U.K., in 1989.

He was a Science and Engineering Research Council Information Technology Fellow with the University of Cambridge, where he worked on all-optical nonlinearities in waveguide devices. He is currently the Professor of Photonics at the University of Cambridge, having previously held academic posts at the University of Bath, Bath, U.K., and the University Bristol, Bristol, U.K. He has been the author of more than 500 refereed journal and conference papers. His research interests include high-speed optical communications systems, wavelength conversion, and wavelength-division multiplexing networks, optical amplifiers, optical nonlinearities for switching applications, and high-power semiconductor lasers.

Prof. Penty is the Editor-in-Chief of the *IET Optoelectronics Journal*.

Ian H. White (S'82–M'83–SM'00–F'05) received the B.A. and Ph.D. degrees from the University of Cambridge, Cambridge, U.K., in 1980 and 1984, respectively.

He was appointed as a Research Fellow and an Assistant Lecturer with the University of Cambridge before he became a Professor of physics with the University of Bath, Bath, U.K., in 1990. In 1996, he moved to the University of Bristol, Bristol, U.K., where he was a Professor of optical communications, the Head of the Department of Electrical and Electronic Engineering in 1998, and the Deputy Director of the Centre for Communications Research. He returned to the University of Cambridge in October 2001 as a van Eck Professor of engineering. He is currently the Head of Photonics Research with the University of Cambridge. He is the author of more than 800 publications and the holder of 28 patents.

Prof. White is currently a Member of the Board of Governors of the IEEE Photonics Society and Editor-in-Chief of *Electronics Letters*.